



**HAL**  
open science

# Stratigraphic Control of Frontal Décollement Level and Structural Vergence and Implications for Tsunamigenic Earthquake Hazard in Sumatra, Indonesia

Kyle Bradley, Yanfang Qin, Helene Carton, Nugroho Hananto, Fernando Villanueva-robles, Frédérique E Leclerc, Wei Shengji, Paul Tapponier, Kerry Sieh, Satish C Singh

## ► To cite this version:

Kyle Bradley, Yanfang Qin, Helene Carton, Nugroho Hananto, Fernando Villanueva-robles, et al.. Stratigraphic Control of Frontal Décollement Level and Structural Vergence and Implications for Tsunamigenic Earthquake Hazard in Sumatra, Indonesia. *Geochemistry, Geophysics, Geosystems*, 2019, 20 (3), pp.1646-1664. 10.1029/2018GC008025 . hal-02192779

**HAL Id: hal-02192779**

**<https://hal.science/hal-02192779>**

Submitted on 10 Nov 2020

**HAL** is a multi-disciplinary open access archive for the deposit and dissemination of scientific research documents, whether they are published or not. The documents may come from teaching and research institutions in France or abroad, or from public or private research centers.

L'archive ouverte pluridisciplinaire **HAL**, est destinée au dépôt et à la diffusion de documents scientifiques de niveau recherche, publiés ou non, émanant des établissements d'enseignement et de recherche français ou étrangers, des laboratoires publics ou privés.



Distributed under a Creative Commons Attribution - NoDerivatives 4.0 International License



## RESEARCH ARTICLE

10.1029/2018GC008025

### Key Points:

- We present seismic reflection and bathymetry data for the Sumatran accretionary wedge offshore of the Mentawai islands, Sumatra, Indonesia
- The vergence of frontal wedge thrusts is closely related to the stratigraphic level of the shallow decollement
- Enhanced near-trench slip during 2010 Mentawai earthquake corresponds with frontal bivergence and a decollement rooted in Miocene sediments

### Correspondence to:

K. Bradley,  
kbradley@ntu.edu.sg

### Citation:

Bradley, K., Qin, Y., Carton, H., Hananto, N., Villanueva-Robles, F., Leclerc, F., et al. (2019). Stratigraphic control of frontal décollement level and structural vergence and implications for tsunamigenic earthquake hazard in Sumatra, Indonesia. *Geochemistry, Geophysics, Geosystems*, 20, 1646–1664. <https://doi.org/10.1029/2018GC008025>

Received 18 OCT 2018

Accepted 7 MAR 2019

Accepted article online 14 MAR 2019

Published online 29 MAR 2019

©2019. The Authors.

This is an open access article under the terms of the Creative Commons Attribution-NonCommercial-NoDerivs License, which permits use and distribution in any medium, provided the original work is properly cited, the use is non-commercial and no modifications or adaptations are made.

## Stratigraphic Control of Frontal Décollement Level and Structural Vergence and Implications for Tsunamigenic Earthquake Hazard in Sumatra, Indonesia

Kyle Bradley<sup>1,2</sup> , Yanfang Qin<sup>3</sup> , Hélène Carton<sup>3</sup> , Nugroho Hananto<sup>4</sup> , Fernando Villanueva-Robles<sup>1,3</sup> , Frédérique Leclerc<sup>5</sup> , Wei Shengji<sup>1,2</sup> , Paul Tapponnier<sup>1,2</sup> , Kerry Sieh<sup>1,2</sup> , and Satish Singh<sup>1,3</sup>

<sup>1</sup>Earth Observatory of Singapore, Nanyang Technological University, Singapore, <sup>2</sup>Asian School of the Environment, Nanyang Technological University, Singapore, <sup>3</sup>Equipe de Géosciences Marines, Institut de Physique du Globe de Paris (CNRS, Paris Diderot, Sorbonne Paris Cité), Paris, France, <sup>4</sup>Now at Research Center for Deep Sea, Indonesian Institute of Sciences, Ambon, Maluku, Indonesia, <sup>5</sup>Géoazur, Université Nice Sophia Antipolis (Université Côte d'Azur, CNRS, IRD, Observatoire de la Côte d'Azur), Valbonne, France

**Abstract** Propagation of fault rupture to the seafloor is a likely cause of enhanced tsunami generation during megathrust earthquakes. New, high-resolution seismic reflection profiles and swath bathymetry collected across the northern limit of the  $M_w$  7.8, 25 October 2010 Mentawai tsunami earthquake rupture reveal significant and systematic lateral variations in both the stratigraphic level of the frontal Sunda megathrust and the vergence of its frontal ramp faults. Where ramp faults are uniformly seaward vergent, the décollement resides on top of a strong reflector marking the inferred top of pelagic sediments. Where ramp faults are bivergent (both landward and seaward), the décollement is localized within the subducting clastic sequence, above a seismically transparent unit inferred to be distal fan muds. Where ramp faults are uniformly landward vergent, the décollement is directly on top of the oceanic crust of the subducting Investigator Fracture Zone. Enhanced surface uplift and tsunamigenesis during the 2010 tsunamigenic earthquake appear to have coincided with propagation of rupture into frontal areas with well-developed structural bivergence. Frontal bivergence is a geological signal of low basal traction during accrual of slip, and offshore of Sumatra this structural style may mark areas of enhanced tsunami hazard posed by small-magnitude, shallow megathrust ruptures that propagate into the incoming terrigenous sequence at near-trench levels.

**Plain Language Summary** Very large magnitude subduction earthquakes commonly produce huge tsunamis that devastate shorelines great distances away from the source. These tsunamis are generally preceded by strong ground shaking that warns coastal residents near the rupture area to evacuate. Over the last several decades, the subduction zone south of Sumatra and Java has produced three deadly tsunamis that were caused by much smaller-magnitude earthquakes. The high casualty count of these events, called tsunamigenic earthquakes, is largely due to the lack of warning from major ground shaking before arrival of the tsunami waves. The cause of these earthquakes remains poorly understood and few studies have directly examined the fault systems that produce the excessively large waves. We used seismic reflection and bathymetry data to study an area of the Sumatran subduction zone that produced a tsunamigenic earthquake in 2010 and killed more than 500 people. We focused on understanding the different kinds of rock the shallowest megathrust fault cuts through, which might have different frictional properties. By comparing the stratigraphic position of the fault with the geological structure of the overlying wedge, we show that excessive slip occurred in a specific geological context that indicates low friction on the fault surface. This is a significant step in better understanding how tsunamigenic earthquakes happen in this region.

### 1. Introduction

The  $M_w$  7.8, 25 October 2010 Mentawai islands earthquake killed more than 500 people living on the forearc island chain offshore central Sumatra when deep coastal inundation by tsunami waves was unheralded by strong ground shaking (Hill et al., 2012; Newman et al., 2011; Satake et al., 2013). Similarly destructive local tsunamis sourced by relatively small magnitude earthquakes struck the southern coast of Java in 1994

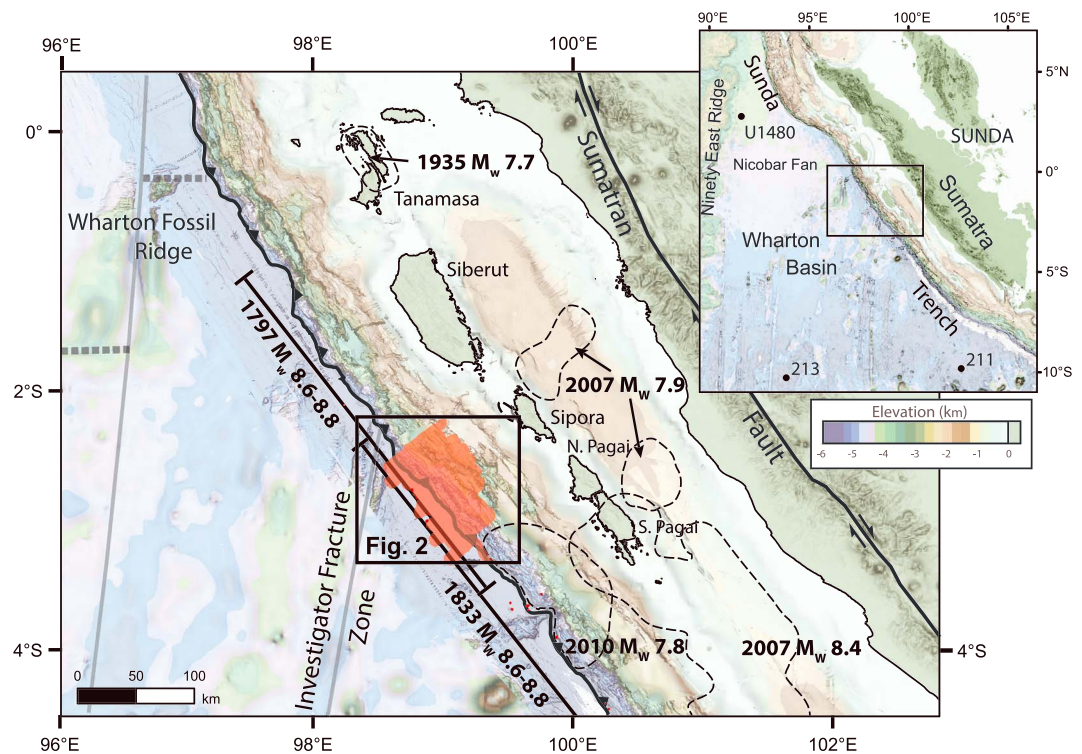


**Figure 1.** Tectonic setting of the Mentawai islands, Sumatra, Indonesia. Eastern Indian Ocean Deep Sea Drilling Project/Integrated Ocean Drilling Program core locations are shown on area map. Slip patches for instrumentally observed Sunda Megathrust earthquakes are shown with dashed lines, and along-trench rupture extents of eighteenth and nineteenth century great earthquakes are shown with thick lines (Konca et al., 2008; Natawidjaja et al., 2004; Natawidjaja et al., 2006; Zhang et al., 2015). The MegaTera study area is shaded red.

(Abercrombie et al., 2001) and 2006 (Lavigne et al., 2007). Such events, termed tsunamigenic earthquakes, are a primary hazard of the Sunda megathrust. Whereas transoceanic tsunamis sourced by huge megathrust earthquakes, such as the 26 December 2004  $M_w$  9.2 Sumatran-Andaman earthquake and the 11 March 2011  $M_w$  9.0 Tōhoku earthquake (Ide et al., 2011), pose a clear hazard to coastal communities, the threat posed by tsunamigenic earthquakes remains poorly understood. This knowledge gap is largely due to uncertainties in the physical mechanisms causing seafloor uplift during shallow megathrust earthquakes.

Propagation of coseismic slip onto the shallowest areas of subduction thrust faults and into the shallow wedge is a likely cause of many surprisingly large tsunami waves (Kanamori, 1972; Polet & Kanamori, 2000). While this process was once considered somewhat unlikely due to presumed stable sliding conditions of faults at shallow depth (Hyndman et al., 1997), plausible mechanisms have been proposed to explain propagation of shallow coseismic slip. These include momentum effects such as dynamic overshoot (Ide et al., 2011), physical effects such as dynamic weakening via thermal overpressurization (Faulkner et al., 2011; Noda & Lapusta, 2013), and/or the influence of the free surface of the shallow wedge during rupture propagation (Gabuchian et al., 2017; Kozdon & Dunham, 2013). It is now widely accepted that rupture can propagate to the trench during great earthquakes ( $M_w$  8.5+) even if the shallow megathrust is velocity strengthening and cannot itself nucleate ruptures. However, the specific mechanisms of seafloor uplift that produce outsize tsunami waves during shallow earthquakes remain uncertain. Here, we seek to improve our understanding of the context of tsunamigenic earthquakes offshore of central Sumatra by documenting in detail the structure and stratigraphic architecture of a hundred kilometer long section of the shallow Sunda megathrust offshore of the Mentawai island chain (Figure 1).

In the vicinity of the study area, frictional locking of the Sunda megathrust extends to a depth of ~40 km and ruptures of the deep locked patch are common (Chlieh et al., 2008; Lange et al., 2018; Prawirodirdjo et al., 2010). Paleogeodetic, historical, and instrumental records of earthquakes reveal that in this region the

megathrust tends to rupture in supercycles of slip events rather than during single throughgoing ruptures like the 2004 Sumatra-Andaman earthquake (Natawidjaja et al., 2006; Philibosian et al., 2014; Philibosian et al., 2017; Sieh et al., 2008). A sequence of two large megathrust earthquakes in 2007 resulted from complex ruptures of the frictionally locked plate interface but did not propagate to shallow levels and did not generate significant tsunami waves (Konca et al., 2008). Increased stress on the updip area of the megathrust following these events may have caused the 2010 Mentawai earthquake (Hill et al., 2012). Few of these large earthquakes have geological or historical evidence for large tsunamis, and the paleogeodetic data do not constrain whether slip propagated to the surface during individual events (Philibosian et al., 2017). If propagation of rupture to shallow levels during great earthquakes that rupture the deep locked patch is uncommon in this area, shallower tsunamigenic ruptures may be more common here. This area is therefore of special interest in terms of hazards posed by tsunamigenic earthquakes.

The geological structure of the upper and lower plates of the shallow megathrust determines the mechanical context, and likely the coseismic slip behavior, of near-surface rupture along the plate interface. Here, we briefly review the main geological features that are most relevant to the structure of the shallow megathrust in our study area.

## 2. Regional Setting and Stratigraphic Context

### 2.1. Geology of the Upper Plate

The leading edge of the upper plate of the Sumatran subduction zone consists of a well-developed accretionary prism derived primarily from accreted sediments. The prism is locally subaerially exposed along the non-volcanic Sumatran forearc ridge and is separated from the mainland by a chain of deep forearc basins that isolate the frontal accretionary wedge from significant terrestrial sediment input (Figure 1). While subduction offshore central Sumatra is oblique ( $\sim 30^\circ$ ) relative to Sunda (Fitch, 1972), the actual obliquity of underthrusting beneath the forearc wedge in this area is smaller ( $\sim 12^\circ$ ) due to partitioning of  $\sim 15$  mm/year of right-lateral slip onto the Sumatran Fault system, a major plate boundary fault that separates the forearc sliver plate from Sunda (Bradley et al., 2017; McCaffrey, 1991).

### 2.2. Geology of the Incoming Indian-Australian Plate

The Eastern Indian Ocean crust is marked by a variety of bathymetric prominences, some of which impinge on the trench and are being subducted. Along the entire Sumatran margin, the most prominent features are approximately north-south oriented fracture zones that formed during Cretaceous through Eocene spreading along the now extinct Wharton Ridge (Jacob et al., 2014). The Investigator Fracture Zone, consisting of four parallel ridge complexes rising up to  $\sim 1$  km above the surrounding seafloor (Liu et al., 1983), forms the western edge of our study area. Plate reconstructions constrained by oceanic magnetic anomalies indicate a latest Cretaceous age for the oceanic crust bordering the deformation front on the eastern side of the Investigator Ridge (Jacob et al., 2014). Isolated, conical volcanic seamounts with up to 2 km of bathymetric relief may belong to the Late Cretaceous to Paleogene CHRISP seamount province (Hoernle et al., 2011).

The sedimentary cover of the incoming plate hosts the shallowest megathrust and is therefore a critical factor for its mechanical behavior. While direct observations have not been made within our study area, the regional stratigraphy has been documented by sparse coring. Drilling records of Wharton Basin sediments are available from three locations broadly bracketing the study area (Figure 1, inset). Integrated Ocean Drilling Program Leg 362 cores U1480 and U1481 were sited within the northwestern Wharton Basin in the vicinity of the Ninety East Ridge, proximal to sources of Himalayan-derived sediment that make up the Nicobar Fan (McNeill, Dugan, Backman, et al., 2017; McNeill, Dugan, Petronotis, et al., 2017). Deep Sea Drilling Project Leg 22 drilled with periodic coring into the top of the oceanic crust at sites 211 and 213 in the southern Wharton Basin, where the Nicobar Fan clastic sequence is thinner (von der Borch et al., 1974).

In each of these cores, basal calcareous and volcanoclastic sediments record deposition in the vicinity of the active spreading ridge, above the carbonate compensation depth. Overlying claystone horizons record deep water sedimentation in a low-productivity ocean setting. These low accumulation rate sediments are overlain by a terrigenous clastic sequence sourced from the Himalayan collision zone, comprised of turbiditic sands, silts, and muds. Following the end of active clastic sedimentation on the Nicobar Fan, the Wharton

Basin was blanketed by thin nannofossil clays and ashes (McNeill, Dugan, Backman, et al., 2017). Based on this regional information, the incoming oceanic crust in our study area is expected to be directly overlain by a variegated pelagic sequence that is in turn covered by distal and then more proximal turbiditic sediments of the Nicobar Fan, and finally a second, thin pelagic sequence. Near the trench, material derived from mass wasting of the sediment-starved accretionary wedge is expected to overlie the incoming lower plate stratigraphy.

### 3. Seafloor Morphology From Swath Bathymetry

The data used in this study were collected onboard the Schmidt Ocean Institute's *R/V Falkor* as part of the MegaTera (Mentawai Gap Tsunami Risk Assessment) project. Our study area encompasses 114 km of the subduction trench immediately east of the Investigator Fracture Zone and extends 50 km onto the lower inner slope, and up to 20 km onto the outer slope (Figures 1 and 2). We collected swath bathymetry simultaneously with seismic data using a SIMRAD EM302 multibeam echo-sounder system with an operating frequency of 30 kHz, producing an effective resolution at 4-km water depth of 4–5 m vertical and 25 m horizontal. The swath width at these water depths is 7.5 km, and hence, the line spacing was 6 km, allowing overlapping coverage of the seafloor. The bathymetry data were processed on board using CARIS HIPS software and gridded at 25 × 25 m.

The bathymetric trench is located between 5 and 20 km from the deformation front, and separates a gently sloping (2.5°) outer rise from a more steeply sloping (4–5°) accretionary wedge (Figure 3a). The bathymetric trench deepens toward the southeast, indicating the dominant direction of along-trench sediment transport, and the bathymetric low is locally deflected westward away from the wedge by sedimentary fans sourced from the collapsing prism. The most frontal deformational structures of the accretionary wedge are low-amplitude, uneroded folds that uplift and deflect channels that drain the accretionary wedge and which sourced the frontal fans. The frontal ridges have planar to slightly convex-upward crests, exhibit low degrees of dissection, and are tilted either landward or seaward. In the northern study area (Figure 3b), the tilt is generally toward the trench, while in the central study area (Figure 3c) it is away from the trench. In the southern study area (Figure 3d), juvenile fold crests are tilted in both directions, as has been seen elsewhere along the Sumatran margin (Frederik et al., 2015). Slide blocks up to 1 km wide occur in a few locations ahead of the deformation front, but larger landslide deposits are absent. Over much of the study area, higher-elevation folds are marked by increasingly dissected ridges that impound underfilled and internally drained slope basins. The bathymetric relief is rugged, and sediments derived from the forearc islands do not reach to the trench.

### 4. Multichannel Seismic Reflection Imaging

We collected multichannel seismic-reflection data using a single 1.2-km-long seismic streamer with a 12.5-m receiver spacing towed at a water depth of 4.5 m. The source was a two G-gun parallel cluster with total air-gun volume of 500 cubic inches (8.2 L), operated at 2,000 psi, and fired every 25 m. The seismic records had a length of 12 s and a sampling rate of 2 ms. The airguns were deployed at a water depth of 3 m to generate source frequencies up to 200 Hz in order to image fine structure of the shallow subsurface. The vessel speed was ~8.3 km/hr.

Seismic data processing followed a standard workflow. The data were binned in common midpoint gathers every 6.25 m, and swell noise and noisy traces were removed. After velocity analysis, the normal moveout correction was applied and the data were stacked, followed by poststack time migration. Due to the large water depth near the trench (~5 km), the seafloor multiple does not interfere with the structure imaged within the shallow wedge. Because the short streamer provides little information about seismic velocities, the profiles were depth converted using an a priori velocity model developed from multiple long-streamer profiles across the Mentawai wedge, including profile CGG10, which is collocated with line FK30 (Qin & Singh, 2018). This velocity model accounts for an increase in sediment velocity both with burial depth and downdip distance from the deformation front (larger degree of tectonic shortening). The horizontal trace spacing of the resulting data is 6.25 m, and the vertical resolution at a frequency of 100 Hz is 4 m. Profiles were surface muted and gain corrected for display and interpretation. A total of twenty ~40-km-long



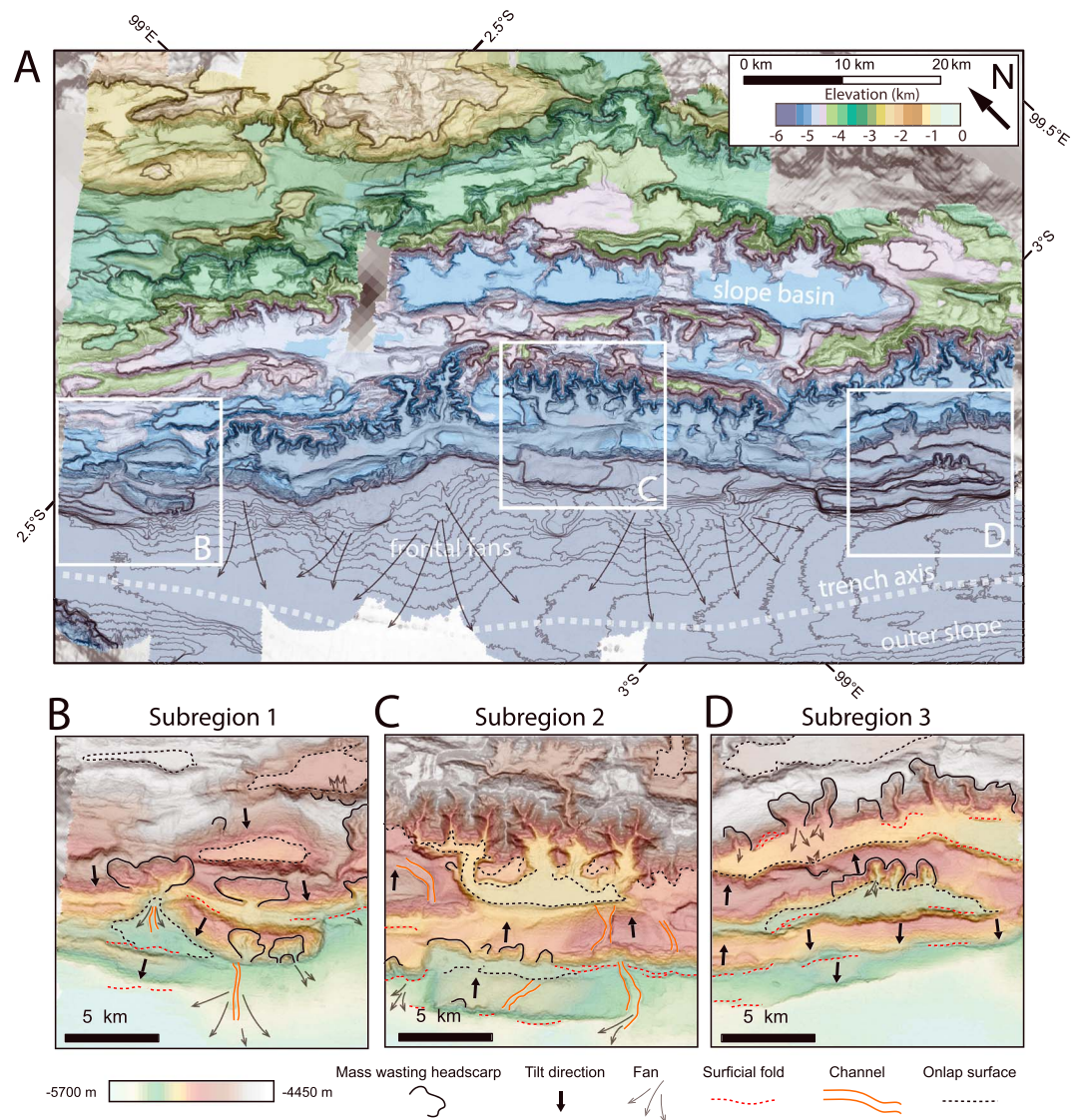


**Figure 3.** Seafloor morphology interpreted from high-resolution bathymetry. Inset boxes have alternative color scale to emphasize the details of the bathymetric relief near the deformation front. Terrain is visualized using a combination of hillshade and surface slope. (a) Overview of the study area; contour interval below  $-5,500$ -m depth is 10 m, above  $-5,500$ -m depth is 1 m; (b) morphology of exclusively landward vergent frontal wedge; (c) morphology of dominantly seaward vergent frontal wedge; and (d) morphology of the bivergent frontal wedge.

Seismic Unit II is characterized by a mostly acoustically transparent interval with variably developed but laterally continuous planar-parallel reflectivity (Figures 4 and 5). It varies in thickness from a maximum of  $\sim 450$  m in the center of the study area to  $\sim 50$  m in the south and is absent from the incoming plate north of FK26, where it pinches out against the Investigator Fracture Zone. The contact with overlying Unit III is typically a high-amplitude reflector, which in some areas exhibits positive polarity (e.g., FK18) and in other areas exhibits clear negative polarity (e.g., FK11–FK14). The high-amplitude reflector at the top of Unit II extends far west of the bathymetric trench and is sharply offset by bending-moment normal faults.

We interpret Unit II as heterolithic pelagic sediments deposited onto oceanic crust. High-amplitude negative polarity (HANP) reflectors such as the one found locally at the top of Unit II have previously been imaged at the top of the basal pelagic sequence along the northern Sumatran subduction system (Dean et al., 2010; Qin & Singh, 2017) and are thought to reflect overpressurization of porous rocks by fresh water released during clay diagenesis (Hupers et al., 2017; Qin & Singh, 2017). The average thickness of Unit II is similar to the

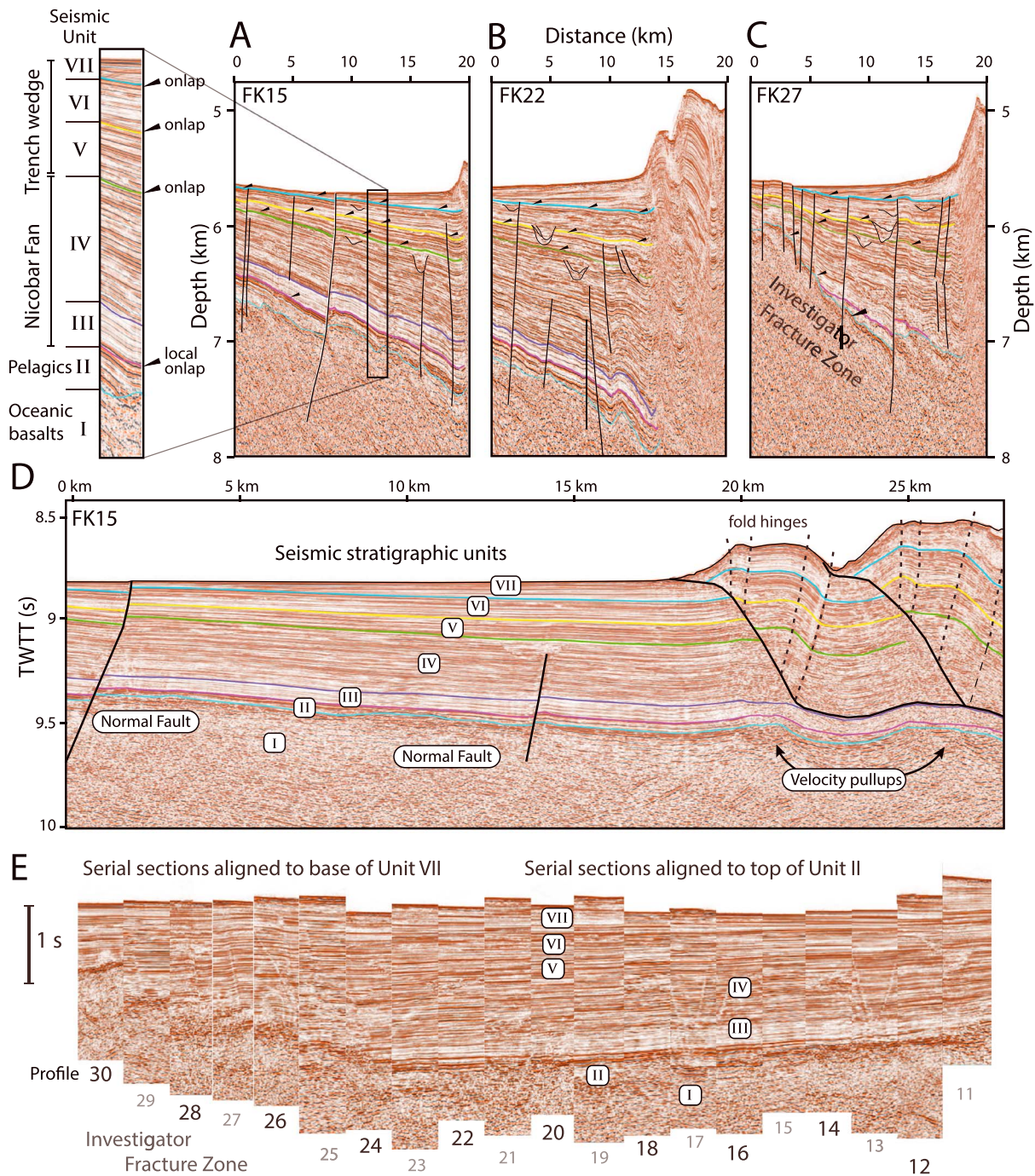


**Figure 4.** Seismic stratigraphy of the incoming plate interpreted from depth-converted profiles. Panels (a)–(c) have 10 times vertical exaggeration. (a) Southernmost profile FK15 shows a well-developed acoustically transparent interval (Unit III) overlying thin, transparent pelagic sediments (Unit II). (b) Central profile FK22 shows a thinner Unit III overlying a thicker and more reflective Unit II. (c) Northern profile FK27 shows lateral pinch-out of all stratigraphic units against the basement relief of the Investigator Ridge. (d) Time domain seismic profile showing seismic character of Units I–VII. Velocity pull-ups beneath ramp anticlines are artifacts. Fold hinges are dashed and faults are solid lines. (e) Lateral stratigraphic variation seaward of the deformation front shown by serial seismic sections.

thickness of pelagic sediments penetrated by Integrated Ocean Drilling Program core U1480 (McNeill, Dugan, Backman, et al., 2017) and imaged on seismic lines within the Wharton Basin (Carton et al., 2014; Dean et al., 2010).

Seismic Unit III is characterized by planar-parallel to slightly wavy reflectors without internal truncations. This unit is in most places conformable with Unit II, but in several basement lows it does onlap onto tilted

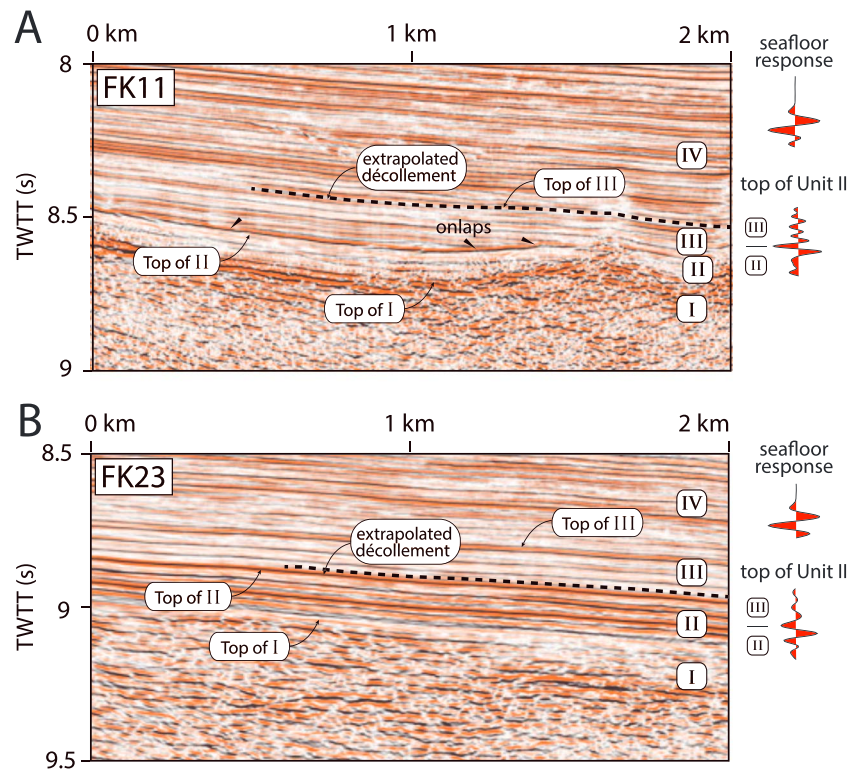


**Figure 5.** Along-strike variation of the basal stratigraphy of the incoming plate. Line locations are given on Figure 2. The position of the décollement is extrapolated from structural interpretations. Stacked seismic traces show the response of the seafloor and of the Unit II/Unit III contact. (a) Profiles FK11–FK18 show a thin, transparent pelagic sequence onlapped by Unit III and capped by a high-amplitude, commonly negative polarity reflector. Unit III is seismically transparent, with subvertical linear disruptions of reflection intensity that do not extend into Unit IV. (b) Profiles FK16–FK25 show a thicker pelagic sequence defined by high-amplitude, continuous reflectors. TWTT = two-way travel time.

Unit II reflectors (Figure 5a), indicating a depositional hiatus. Unit III is 150–200 m thick in the south (FK12) but thins dramatically northward, disappearing as a recognizable unit around profiles FK19 and FK20.

We interpret Unit III as outer fan hemipelagic muds of likely middle Miocene age. Its seismically semitransparent character, laterally continuous and evenly spaced reflectors, and lack of channeling are similar to seismic reflection features of hemipelagic muds imaged at the base of the Nicobar Fan (McNeill, Dugan, Backman, et al., 2017), as well as deep water hemipelagic muds that have been imaged elsewhere (Spinelli & Underwood, 2004).

Seismic Unit IV is the thickest single unit within the study area, varying in thickness between 450 and 700 m. It is conformable and potentially transitional with Unit III. This unit has medium- to high-amplitude, planar-parallel reflectivity. Reflector truncations are limited to fill sequences within buried channels 1–2 km wide and up to 100 m deep.

Unit IV is similar in character of reflectivity and presence of channel complexes to the upper sequence of the Nicobar Fan (McNeill, Dugan, Backman, et al., 2017), and we therefore interpret it as middle fan turbidites. Units III and IV together make up the Nicobar Fan in the study area.

Seismic Units V–VII are a stacked sequence of similar seismic character, with basal acoustically transparent intervals that thin seaward and are overlain by homogeneously reflective, internally parallel to slightly divergent reflectors that exhibit angular discordance with the underlying sediments. These sequences thin toward the forebulge and thicken into the wedge, where they are uplifted in frontal folds and can be correlated across fold structures up to 20 km from the modern deformation front. Eastward thickening and the angular discordances separating Units V–VII indicate deposition in the vicinity of the outer rise and trench, where slab bending occurs. Units V–VII attain a composite thickness of 500–750 m at the deformation front but continue to thicken eastward into the deformed wedge.

We interpret Units V–VII as stacked trench-fill sequences sourced from a combination of along-trench transport and mass wasting of the inner slope. The overall pattern of angular discordance between internally sub-parallel reflectors suggests that these units represent discrete pulses of high sediment flux, possibly moderated by global climate conditions and sea level changes.

### 5.2. Along-Strike Stratigraphic Variations

The close spacing of our seismic profiles allows us to correlate stratigraphic features of the incoming plate along 114 km of the subduction zone (Figures 4d and 4e). The sedimentary section exhibits significant along-strike variation, presenting a diverse environment through which the shallow décollement must eventually propagate. The primary bathymetric feature is the eastern flank of the Investigator Fracture Zone that impinges on the trench between lines FK25–FK30. The Unit II pelagic sequence is notably thicker around the buried ridge, but pinches out against the Investigator Fracture Zone to the north. Thickening of Unit II sediments and their highly reflective character within the central study area, and absence of Unit II on the flank of the Investigator Fracture Zone, is probably due to infilling of a preexisting bathymetric depression by pelagic sediments redistributed by bottom currents. The Nicobar Fan Units III and IV also thin northward and pinch out against the steep eastern flank of the Investigator Fracture Zone (Figure 4e).

## 6. Structural Geology

### 6.1. Normal Faults in the Downgoing Plate

Bending-moment normal faults exhibiting at most several hundred meters of throw are common between the forebulge and the deformation front (Figure 2). The strike of these faults forms a  $\sim 20^\circ$  angle with the strike of the wedge thrusts, cutting across the inferred N-S and E-W structural grains of the oceanic basement (Figure 2). Although some faults are clearly sealed by Units V–VII (Figure 4d), recording slab bending outboard of the trench, others cut the entire incoming stratigraphy and are expressed as sharp scarps at the surface, indicating that slab bending remains active near the trench (e.g., Craig et al., 2014). Despite the common occurrence of these faults in the undisturbed section west of the deformation front, we have identified very few normal faults within the shortened sediments of the accretionary wedge.

### 6.2. Wedge Thrust Vergence

The typical seaward vergence of (landward dipping) thrust faults in accretionary wedges arises primarily by rotation of principal stresses due to basal traction on a frictional décollement (Davis & Engelder, 1985). In contrast, wedges that exhibit simultaneous shortening on both landward and seaward vergent faults, or consistent landward vergence, are characterized by a low basal traction and a low degree of internal stress rotation (Bonini, 2007). Systematic patterns of thrust vergence are therefore potential indicators of spatially variable mechanical properties of the décollement, which might be implicated in shallow rupture scenarios.

In our study area, thrust faults within the upper  $\sim 2$  km are commonly marked in seismic reflection profiles by normal-polarity fault plane reflectors that coincide with reflector truncations (Figure 6a). Thrust and normal faults with small offsets are visible as dipping zones of disrupted reflectivity (Figures 6a and 6b). The high resolution of the seismic data allows us to map the structural vergence of ramp thrusts throughout the frontal wedge. The large and laterally continuous thrust faults that structure the middle slope ( $>25$  km from the deformation front) are primarily seaward vergent thrusts associated with ramp anticlines (Figure 2), although significant structural complexity exists due to thickening of the accretionary wedge by duplexing.

Along much of the Sumatra-Andaman-Java margin and within our study area, the most frontal part of the wedge shows the greatest along-strike structural variability. We identify three distinct regions of systematic ramp fault vergence along the lowermost inner slope, which coincide with the three zones of distinctive surface morphology of frontal folds (Figure 3a). In the northwestern area (Subregion 1; Figure 3b) frontal faults are all landward vergent and imbricate a prism-shaped sedimentary sequence that thins onto the flank of the Investigator Fracture Zone (Figure 7a). Slope basins are absent and the degree of dissection of ramp anticlines is small. Ramp anticlines are separated by 2–3 km, with anticlinal crests sloping toward the trench. This style of deformation is similar to that observed by Cook et al. (2014)  $\sim 300$  km northwest of our study area, where thin sediments overlying the subducting Wharton Fossil Ridge are also imbricated with systematic landward vergence.

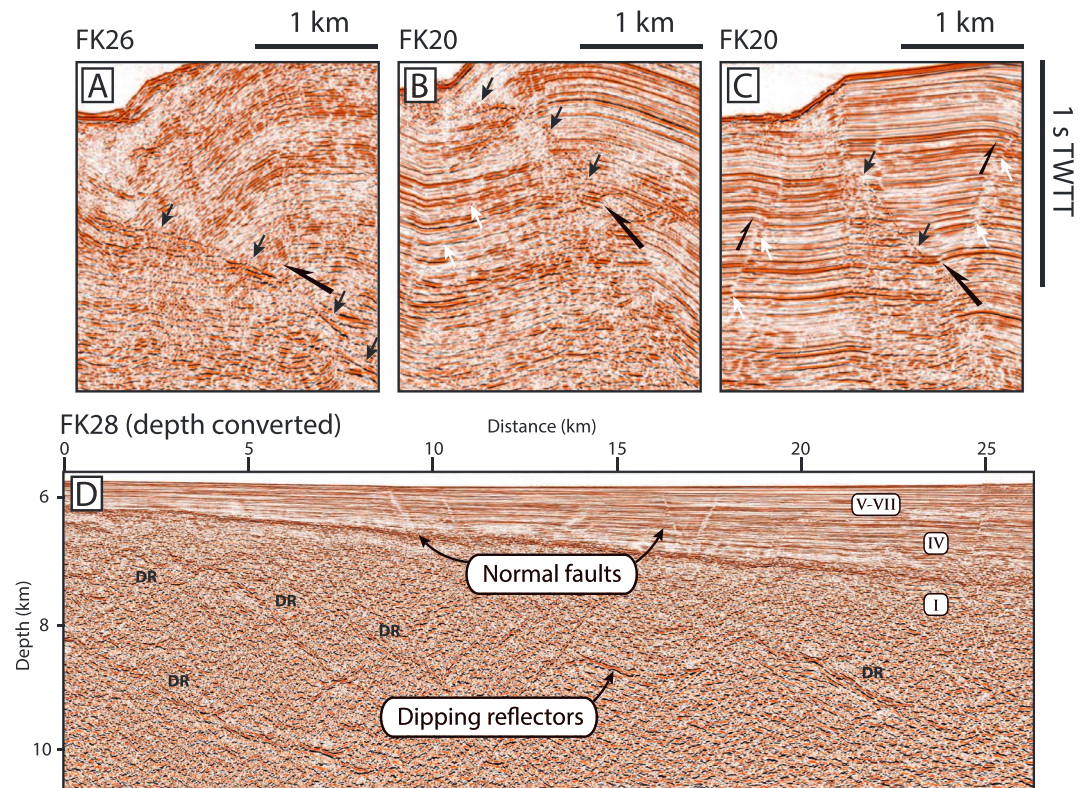


**Figure 6.** (a–c) Three examples of the typical resolution and imaging capability of the seismic reflection profiles. Profile locations are given in Figure 2. Faults are identifiable by fault plane reflectors marking faults with several hundred meters of throw (black arrows) as well as zones of disrupted reflectivity marking faults with less than ~20 m of throw (white arrows). (d) Depth-converted profile showing dipping reflectors within the oceanic crust and lateral pinch-out of sediments against the Investigator Fracture Zone. Small-offset normal faults within the sediments appear as zones of decreased imaging. TWTT = two-way travel time.

In the central area (Subregion 2; Figure 3, FK20–FK26), frontal thrusts are dominantly seaward vergent, with only a few small landward vergent thrusts that root onto seaward vergent ramps and not the décollement (Figure 7b). Large ramp anticlines are separated by ~5 km, are strongly dissected, and impound partially filled slope basins. Laterally discontinuous, low ridges on the landward slope close to the trench mark the early formation stage of ramp anticlines along the leading edge of incoming basement relief. Such seaward vergence is characteristic of most of the wedge thrusts that cut the Andaman-Sumatra-Java prism, with significant exceptions where frontal thrusts are either landward vergent or bivergent (Frederik et al., 2015; Graindorge et al., 2008; McNeill & Henstock, 2014; Moeremans et al., 2014).

In the southeastern part of the study area (Subregion 3), frontal faults are bivergent, exhibiting similar amounts of total slip on oppositely vergent thrusts (Figure 7c). Frontal ramp anticlines are separated by 3–5 km, show either landward or seaward tilt, and are not strongly dissected (Figure 3d).

The lateral transitions between these three subregions are abruptly defined by interfingering fault and fold terminations and lateral steps in the location of the décollement tipline, rather than linear tear faults or strike-slip faults. Notably, there appears to be a close correspondence between the seaward vergent thrusting and the existence of a reflective Unit II pelagic sequence overlying Unit I oceanic crust and landward vergent thrusting where the décollement resides at the top of Unit I oceanic crust (Figure 8). The northward transition from seaward to landward vergence closely tracks the northward pinch-out of subducted Unit II. This correlation holds in detail even within each reflection profile: in profiles dominated by seaward vergent ramp thrusts, small topographic prominences of oceanic crust around which Unit II is ponded are marked by landward vergent thrusts, some of which are incipient (e.g., profile FK26; Figure 8).

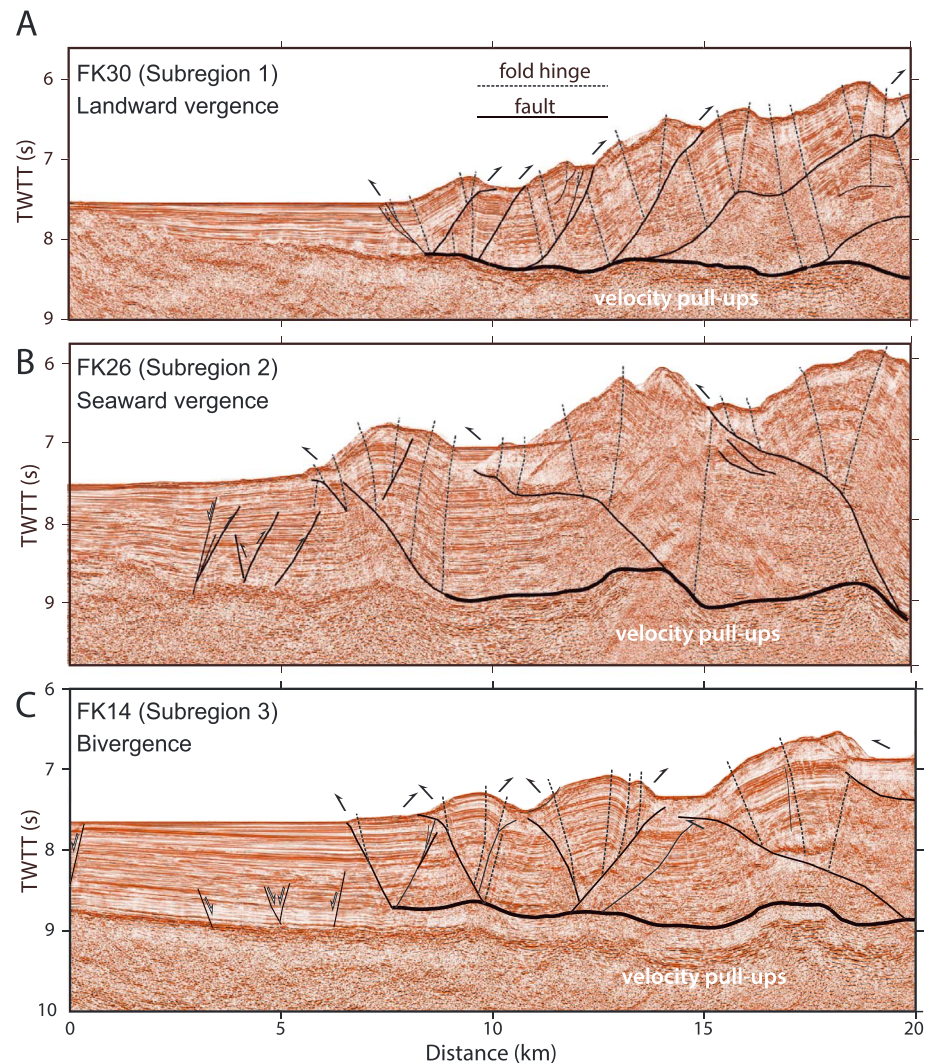


**Figure 7.** Interpreted time domain seismic reflection profiles representative of the three structural domains identified in this study, showing the inferred décollement (thick black lines), ramp thrusts (thin black lines), and fold hinges (dashed lines). Velocity pull-ups occur beneath anticlines. (a) Line FK30 shows consistent landward vergence. (b) Line FK26 shows consistent seaward vergence. (c) Line FK14 shows structural bivergence. TWTT = two-way travel time.

### 6.3. Wedge Geometry and Distribution of Active Shortening

The spatial distribution of coseismic surface uplift is an important factor for tsunamigenesis. While a critically stressed wedge might simultaneously activate a large number of frontal ramp faults during a tsunamigenic earthquake (Wang & Hu, 2006), some actively accreting wedges are known to accommodate most of their shortening budget only on a few frontal structures (Pedley et al., 2010). While remote geophysical observations cannot directly resolve pattern of tsunamigenic surface uplift along the most frontal reaches of the megathrust (Hill et al., 2012), seismic reflection profiles can directly constrain the long-term proportion of geological slip distributed across frontal ramp faults.

In our study area, seaward vergent thrusts exhibit a steep ( $\sim 45^\circ$ ) ramp at depth and a more shallowly dipping ( $0\text{--}10^\circ$ ) flat near the surface (Figure 9). This shallow thrust flat marks the preexisting seafloor surface that was covered by debris and then overridden by seaward tilted beds of the frontal ramp anticline. Large amounts of mass wasting have occurred on these oversteepened fold limbs due to detachment of sediments along bedding planes, in places completely isolating the leading edge of the upper plate as erosional remnants that are buried by thin slope basin sediments (Figure 3). The tip of the shallow thrust flat is

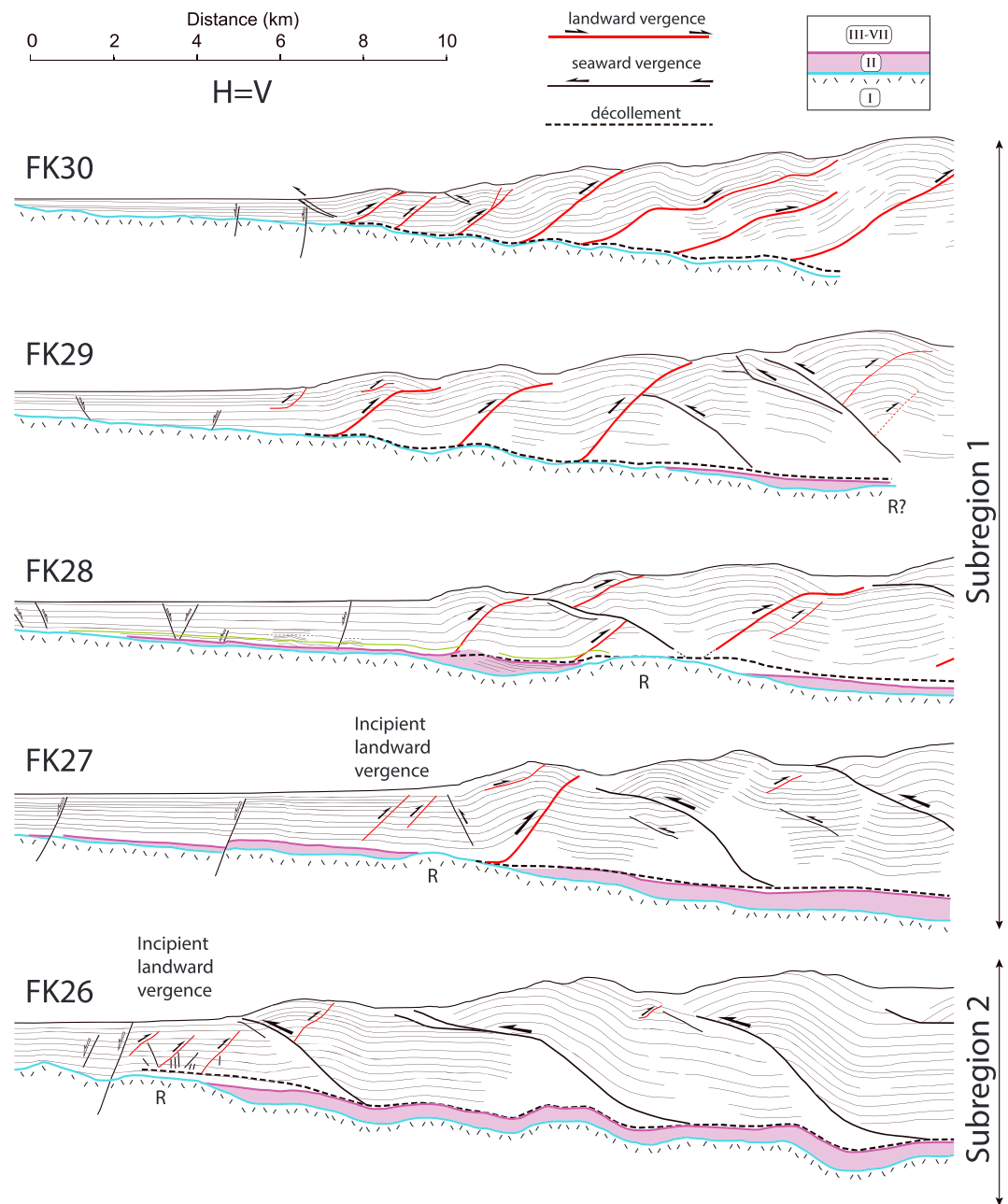


**Figure 8.** Along-strike transition from frontal landward vergence associated with a décollement overlying oceanic crust (Subregion 1, FK27–FK30) to frontal seaward vergence associated with a décollement overlying basal pelagic sediments (Subregion 2, FK19–FK26), from interpretation of depth-converted seismic profiles. There is a clear correlation between both updip and along-strike pinch-out of pelagic sediments and a systematic switch in ramp fault vergence from seaward to landward. The transition from landward to seaward vergence away from the deformation front in Subregion 1 is controlled by the presence of pelagic sediment below the décollement. Nascent landward vergence near the deformation front on lines FK26 and FK27 coincides with thinning or disappearance of pelagic sediments above an incoming prominence of the oceanic crust.

commonly folded by the active hinge of a younger seaward vergent fold. These relationships suggest that only the most frontal ramp faults are accumulating significant slip at present.

Evidence of a systematic break-forward deformation style is also preserved beneath the largest slope basins. There, flat-lying basin sediments lap onto landward tilted beds of buried ramp anticlines and seal the thrust faults underlying the anticlinal forelimbs (Figure 9). The slope basin deposits extend seaward, where they

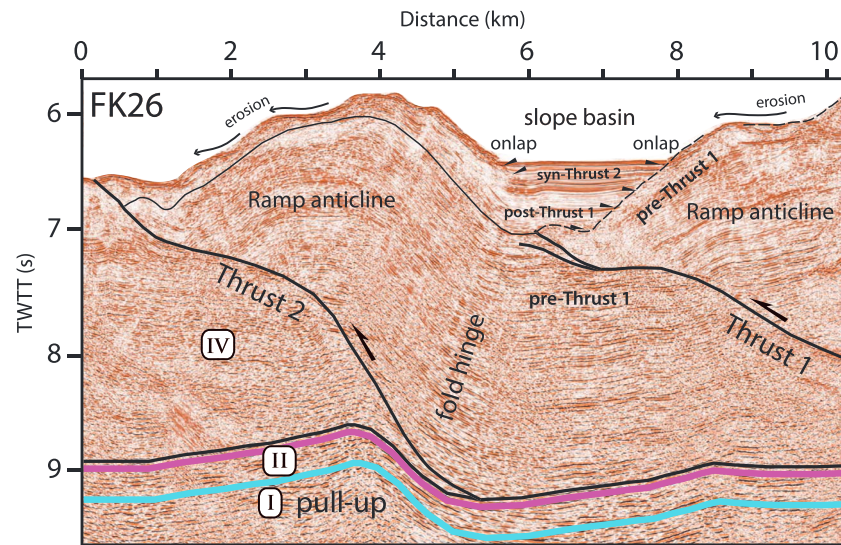


**Figure 9.** Break-forward thrusting exhibited by two seaward vergent ramp thrusts within Subregion 2. Location is given in Figure 2. Thrust 1 and its associated ramp anticline are onlapped by flat-lying slope basin deposits, which are themselves uplifted onto the crest of the ramp anticline of Thrust 2. Postthrust 2 slip on Thrust 1 is small. TWTT = two-way travel time.

are folded and uplifted onto the ramp anticline of the more seaward ramp fault. Recent deformation in the wedge is therefore dominantly break forward, with active shortening being accommodated on the most frontal ramp thrusts and only a very minor amount of out-of-sequence deformation. The largest portion of ramp fault displacement and surface uplift during near-trench coseismic slip should be distributed only onto the one to two most frontal structures. This analysis does not account for potentially hazardous out-of-sequence splay faults that may exist higher within the accretionary wedge (Cook et al., 2014; Kopp & Kukowski, 2003).

#### 6.4. Critical Taper

We mapped the top of Unit I (oceanic crust) on all depth-converted seismic profiles (Figure 10). As our structural interpretations show that the décollement is bedding-parallel in all three vergence domains, we use the oceanic crust reflector as a simple proxy for the dip angle of the décollement. The wedge taper (the sum of the surface slope,  $\alpha$ , and the décollement dip,  $\beta$ ; Dahlen, 1990) varies between  $\sim 9.5^\circ$  and  $11.5^\circ$ . Differences in the inferred taper are within the uncertainties of the surface slope and décollement dip angles and are not significant. While the velocity model we use to depth convert the seismic lines could be inaccurate, the bias would not affect the conclusion of a similar taper in all three structural domains. The consistency of the taper angle across the study area indicates that lateral variations of the frictional strength of the décollement and the internal frictional strength of the wedge are not sufficient to explain the lateral changes in the vergence of the frontal wedge.

### 7. The Stratigraphic Level of the Décollement

While the décollement is not a distinctive seismic reflector, the fault-bend fold geometry of frontal structures allows us to estimate quantitatively the depth of the frontal décollement (Suppe, 1983). Depth-converted seismic lines show that frontal structures in the study area are dominantly flexural slip fault-bend folds defined by a ramp anticline with a well-imaged dip panel separating an active axial surface that bisects the bedding angle from a subparallel inactive axial surface (Figure 11). We use positive polarity ramp fault plane reflectors, fault diffractions, stratigraphic truncations, and bedding cutoff angles to define the position and dip of planar ramp faults. The intersection of the projected fault plane and the active axial surface should correspond with the vertical position of the décollement tipline. While most dip panels are approximately parallel to the ramp fault (FK15 in Figure 11), several frontal anticlines exhibit broad back limbs that dip more shallowly than the ramp fault and active axial surfaces that intersect the décollement at the fault bend; we identify these structures as simple shear fault-bend-folds (FK23 in Figure 11) and also identify the level of

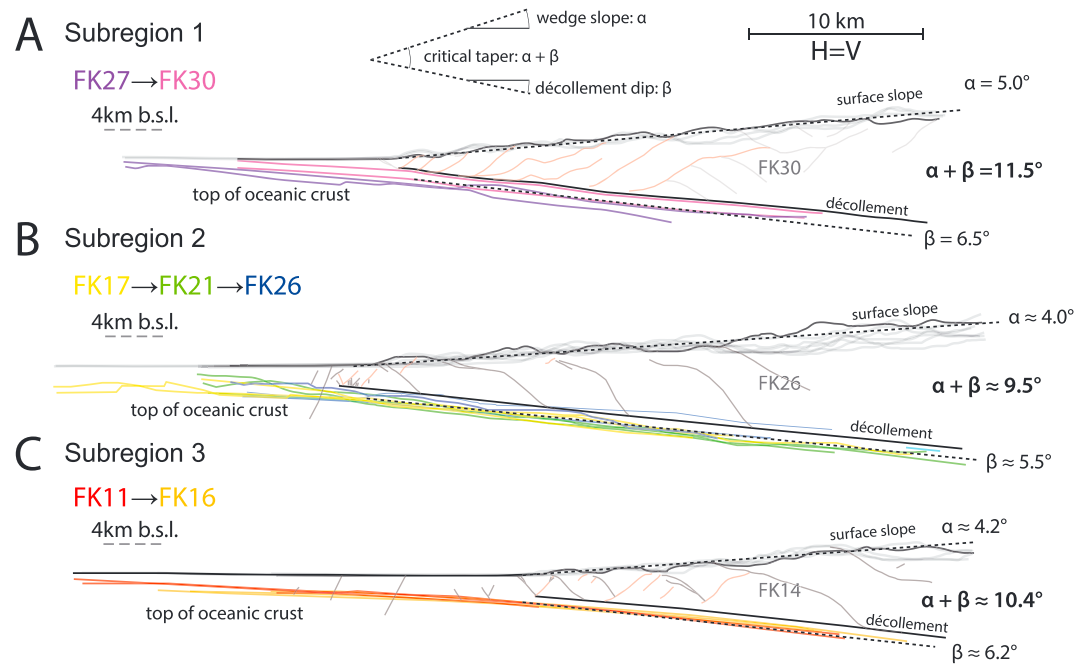


**Figure 10.** Critical wedge tapers of the (a–c) three different structural domains. Colored lines indicate the top of the oceanic crust, a strong reflector that is identifiable in all profiles. The décollement is generalized to represent its stratigraphic level above the oceanic crust within each structural domain. Faults and solid black topographic profiles are from representative lines (FK14, FK26, and FK30).

the décollement from the projected intersection of the ramp fault and active kink band. In some profiles, a consistent level of intersection of nascent doubly vergent frontal structures also defines the position of the décollement.

While some active axial surfaces are imaged as tight planar kink bands, most structures exhibit arcuate hinges, introducing uncertainty in the inferred level of the décollement. We therefore utilize the full range of allowable bedding bisector axial surfaces, resulting in an equivalent range in inferred décollement tipline depth. The magnitude of this uncertainty is typically between 50 and 200 m, allowing us to confidently resolve the stratigraphic location of the décollement where seismic units are thicker than ~300 m.

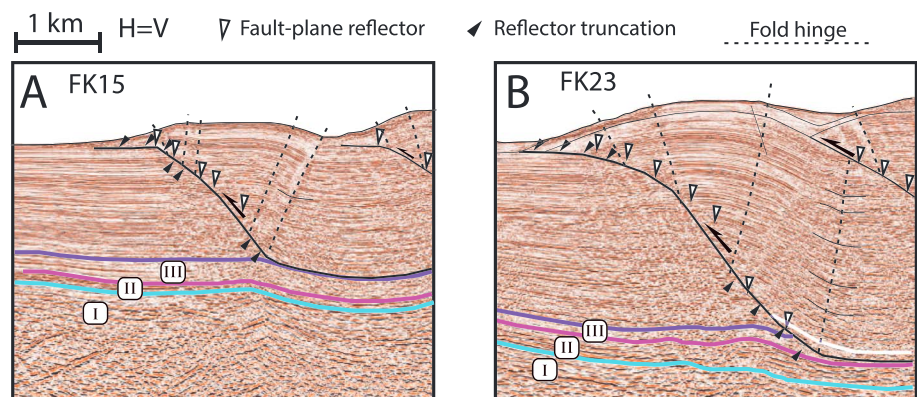


**Figure 11.** Determination of the stratigraphic level of the décollement tipline from fault-bend fold geometries of frontal anticlines on depth-converted profiles. Fault plane reflectors and reflector truncations define the dip and position of the ramp fault (subject to systematic shifts due to migration errors). Hinge lines of the active axial surfaces intersect with the décollement at the take-off location. (a) Line FK15: décollement resides within the Miocene stratigraphy, above Unit III and well above Unit II. (b) Line FK23: décollement resides near the top of a strongly reflective and thick Unit II (pelagic sediments).

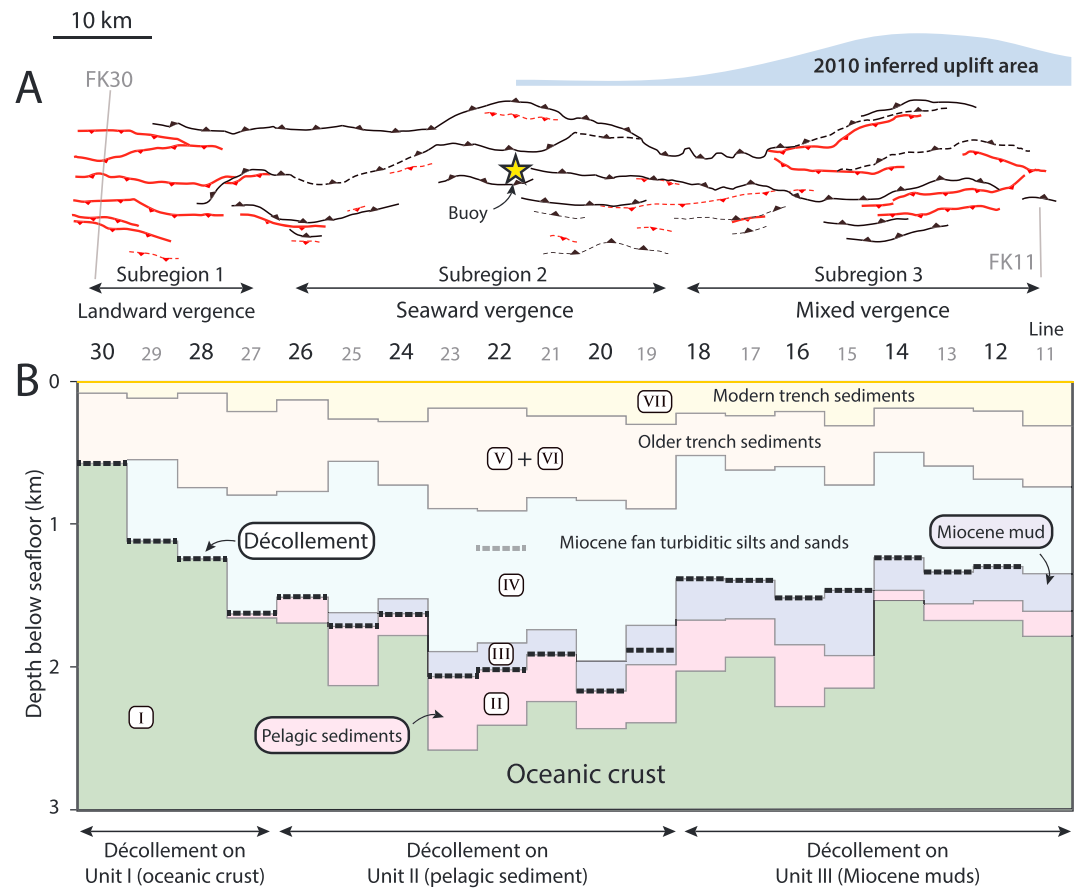


**Figure 12.** (a) Structure map of the study area showing distribution of landward and seaward vergence. (b) Stratigraphic level of the tipline of the décollement. Line-to-line variations in tipline depth are a visual artifact arising from displacement of basement along bending-moment normal faults and along-strike differences in the forward advancement of the décollement tipline. Location of inferred tsunamigenic uplift during the 2010 Mentawai islands earthquake is discussed in the text.

The stratigraphic level of the décollement varies systematically across the study area (Figure 12). In Subregion 1, landward vergent thrusts are rooted into a décollement that sits at the top of the oceanic crust (Unit I). In Subregion 2, seaward vergent thrusts root into a décollement that resides near the top of the pelagic sediment (Unit II; Figure 5b). Finally, in Subregion 3, bivergent thrusts are rooted into a décollement located near the top of Unit III (Figure 5a).

The stratigraphic position of the décollement cannot be identified with confidence farther than 25 km landward from the deformation front due to loss of imaging quality at depth, significant remaining velocity pull-up of reflectors beneath anticlines due to the smooth velocity model used during depth conversion and the increasing effect of imbrication on primary fault dips. However, we nowhere observe thrusting of reflective Unit II onto younger strata within the imaged frontal five to six fold structures, suggesting that the décollement always overlies the pelagic sediments where they are present.

## 8. The 2010 Mentawai Tsunami Earthquake

Waves produced during the 2010 Mentawai tsunami earthquake were monitored by a GITEWS GPS tsunami buoy located directly above the deformation front in the center of our study area (Figure 12). This fortunately located buoy recorded two distinct peaks of sea surface uplift within 5 min of the origin time of the earthquake (Ulutas et al., 2013). Geophysical inversions of fault slip that incorporate buoy and tide gauge data have consistently inferred two separate patches of enhanced seafloor uplift near the trench, corresponding with the first two pulses of GITEWS buoy uplift (Yue et al., 2015, 2014; Satake et al., 2013). A joint inversion

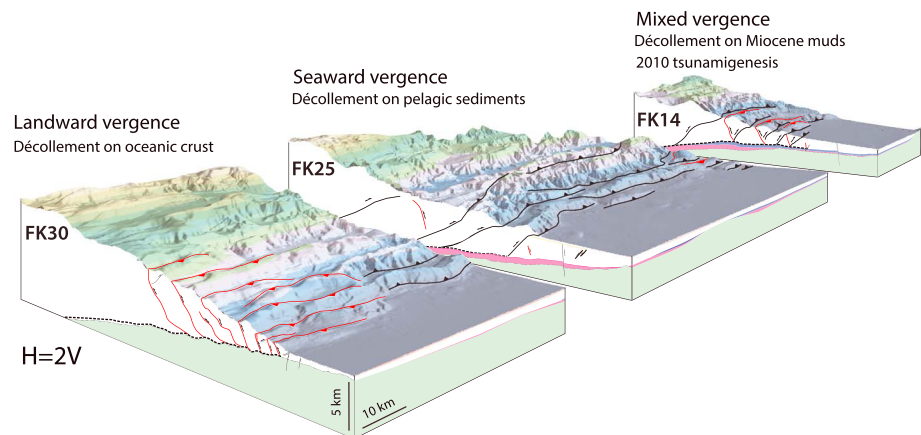


**Figure 13.** Oblique cutaway view of the accretionary wedge in the study area, showing the lateral change in frontal wedge thrust vergence, the stratigraphic level of the frontal décollement, and the relationship to 2010 tsunamigenic uplift.

of buoy and seismic data using nonhydrostatic Green's functions to help resolve near-trench slip also shows that enhanced frontal slip likely did not occur north of  $\sim 3.0^{\circ}\text{N}$  (subfault 12 of Li et al., 2016).

Because the first pulse of sea surface uplift that reached the GITEWS buoy was presumably a direct wave originating from near-trench seafloor uplift near the northwestern termination of rupture, we can roughly estimate the northwestern limit of ground surface uplift from the buoy data. We use a tsunami wave phase velocity of 221 m/s, corresponding with a 5-km average water depth, and assume that the first pulse of buoy uplift was generated by instantaneous near-trench rupture 65 s after the earthquake origin time, consistent with geodetic and back-projection estimates of the rupture duration and propagation (Hill et al., 2012; Lay et al., 2011). Initial uplift of the GITEWS buoy above its background noise level corresponds with inferred uplift along Line FK18; peak uplift corresponds with Line FK14. The inferred uplift decreases south of FK11, corresponding with the subsidence of the buoy after the first peak of uplift. Activation of the frontal faults 10 s earlier would push the inferred location of near-trench uplift farther southeast by only  $\sim 2.2$  km, indicating that the inferred uplift between lines FK11 and FK18 is robust. This basic method of estimating the general area of ground surface uplift is consistent with the nonhydrostatic joint inversion of tsunami measurements from Li et al. (2016).

The inferred area of uplift therefore corresponds with Subregion 3, where frontal ramp faults are bivergent, and confidently excludes Subregion 2. The second pulse of buoy uplift roughly corresponds with another area of bivergent frontal structures located updip of the hypocenter (Li et al., 2016; Satake et al., 2013; Yue et al., 2014). Seafloor uplift and tsunamigenesis during near-trench rupture in 2010 therefore appears to have been enhanced in areas with frontal structural bivergence.

## 9. Discussion and Conclusions

Active shortening in our study area is restricted to the frontal 10–15 km of the wedge. While out-of-sequence thrusting may present a tsunami hazard in this area, as it clearly does in other regions (Bécel et al., 2017; Moore et al., 2007), all lines of evidence currently favor propagation of slip to shallow levels and activation of bivergent frontal structures as the most likely source of excessively large tsunami waves during the 2010 Mentawai earthquake. This is consistent with a primary assumption of models of the tsunami waves; however, the mechanism of surface uplift involves propagation of slip onto ramp faults rather than just the shallowly dipping décollement (Satake et al., 2013; Yue et al., 2014, 2015).

The stratigraphic level of the frontal décollement appears to be intimately related to the frictional properties of the interface, as revealed by lateral changes in structural style that are most readily explained by changes in effective basal friction (Figure 13). Where the décollement overrides Unit III in Subregion 3, basal friction during slip is minor, ramp faults nucleate with both landward and seaward vergence and accrue slip simultaneously. Where the décollement overrides the pelagic sediments of Unit II in Subregion 2, seaward vergence is ubiquitous, indicating stress rotation within the wedge due to stronger basal traction. The

tsunami buoy data indicate that enhanced slip and tsunamigenesis along the northern limit of the 2010 tsunami earthquake arose from Subregion 3, an area where the décollement is localized within the incoming marine fan sequence, above the acoustically transparent Unit III that is interpreted as hemipelagic marine fan muds (Unit III). Dynamic weakening effects associated with this lithological (and possibly hydraulic) boundary are likely responsible for its apparent low friction.

Previous studies of the Sumatran margin have noted dramatic lateral variations in wedge morphology, thickness of the incoming sediments, and style and vergence of wedge faults and folds and have proposed relationships between these features and physical processes that control the propagation of great earthquakes to shallow depth (Cook et al., 2014; Frederik et al., 2015; Graindorge et al., 2008; Gulick et al., 2011; McNeill & Henstock, 2014; Moeremans et al., 2014; Mukti et al., 2012). Our results confirm that significant spatial variations are common and are strongly tied to the geology of the incoming plate.

We confirm that pelagic sediments (Unit II) are subducted at least to shallow depth throughout our study area and that the Unit II–Unit III disconformity commonly hosts the basal décollement. Subduction of pelagic sediments is a common feature of both accretionary wedges and gravity-driven thrust belts (Bilotti & Shaw, 2005; Moore et al., 1990) and may be aided by basal overpressurization due to metamorphic dewatering of clays, as suggested by imaging of a HANP reflector at the top of the incoming pelagic sequence offshore of North Sumatra (Dean et al., 2010; Hupers et al., 2017).

However, stratigraphic units of the incoming Nicobar Fan sequence also locally act as décollement horizons, with significant consequences for the structural style of the wedge and implications for the mechanism of tsunamigenic earthquakes like the 2010 event. Notably, we observe propagation of the décollement into the incoming Miocene sediments overlying a well-defined HANP reflector, indicating that HANP reflectors do not necessarily reflect the preferred level of décollement during its initial formation and propagation. Whether this décollement level persists over time and accommodates subduction of the basal Miocene sequence to greater depths, or whether a lower décollement level eventually develops at the top of the pelagic sequence allowing deeper accretion of the basal Miocene sediments, is not well constrained by the available seismic profiles.

Based on the results of this study, we propose that systematic mapping of ramp fault vergence and the stratigraphic level of frontal décollements in accretionary subduction zones could aid identification of areas of enhanced hazard posed by unexpectedly large tsunami waves. Further observations of frontal accretionary wedges and incoming oceanic stratigraphy in areas that have experienced historical tsunamigenic earthquakes could significantly improve our understanding of the physical mechanisms underlying these damaging events.

#### Acknowledgments

We would like to thank the crew of the R/V Falkor cruise FK150523. We would like to recognize the contributions of Greg Moore, Serge Lallemand, and an anonymous reviewer, which improved the manuscript. Funding for MegaTera was provided by the Earth Observatory of Singapore. The MegaTera expedition was a joint project between the Earth Observatory of Singapore (EOS), the Indonesian Institute of Sciences (LIPI), the Institute de Physique du Globe de Paris (IPGP), and the Schmidt Ocean Institute (SOI). This research is partly supported by the National Research Foundation Singapore and the Singapore Ministry of Education under the Research Centres of Excellence initiative. This work comprises Earth Observatory of Singapore contribution no. 225. High-resolution time domain seismic profiles used in this study are available at the NTU Data Repository (<https://doi.org/10.21979/N9/R1WXXX>). Original marine geophysical data from cruise FK150523 are available from the Marine Geoscience Data System (<https://doi.org/10.7284/901585>).

#### References

- Abercrombie, R. E., Antolik, M., Felzer, K., & Ekstrom, G. (2001). The 1994 Java tsunami earthquake: Slip over a subducting seamount. *Journal of Geophysical Research*, 106(B4), 6595–6607. <https://doi.org/10.1029/2000JB900403>
- Bécel, A., Shillington, D. J., Delescluse, M., Nedimovic, M. R., Abers, G. A., Saffer, D. M., et al. (2017). Tsunamigenic structures in a creeping section of the Alaska subduction zone. *Nature Geoscience*, 10(8), 609–613. <https://doi.org/10.1038/ngeo2990>
- Bilotti, F., & Shaw, J. H. (2005). Deep-water Niger Delta fold and thrust belt modeled as a critical-taper wedge: The influence of elevated basal fluid pressure on structural styles. *AAPG Bulletin*, 89(11), 1475–1491. <https://doi.org/10.1306/06130505002>
- Bonini, M. (2007). Deformation patterns and structural vergence in brittle-ductile thrust wedges: An additional analogue modelling perspective. *Journal of Structural Geology*, 29(1), 141–158. <https://doi.org/10.1016/j.jsg.2006.06.012>
- Bradley, K. E., Feng, L., Hill, E. M., Natawidjaja, D. H., & Sieh, K. (2017). Implications of the diffuse deformation of the Indian Ocean lithosphere for slip partitioning of oblique plate convergence in Sumatra. *Journal of Geophysical Research: Solid Earth*, 122, 572–591. <https://doi.org/10.1002/2016JB013549>
- Carton, H., Singh, S. C., Hananto, N. D., Martin, J., Djajadihardja, Y. S., Udrek, et al. (2014). Deep seismic reflection images of the Wharton Basin oceanic crust and uppermost mantle offshore Northern Sumatra: Relation with active and past deformation. *Journal of Geophysical Research: Solid Earth*, 119, 32–51. <https://doi.org/10.1002/2013JB010291>
- Chlieh, M., Avouac, J. P., Sieh, K., Natawidjaja, D. H., & Galetzka, J. (2008). Heterogeneous coupling of the Sumatran megathrust constrained by geodetic and paleogeodetic measurements. *Journal of Geophysical Research*, 113, B05305. <https://doi.org/10.1029/2007JB004981>
- Cook, B. J., Henstock, T. J., McNeill, L. C., & Bull, J. M. (2014). Controls on spatial and temporal evolution of prism faulting and relationships to plate boundary slip offshore north-central Sumatra. *Journal of Geophysical Research: Solid Earth*, 119, 5594–5612. <https://doi.org/10.1002/2013JB010834>
- Craig, T. J., Copley, A., & Jackson, J. (2014). A reassessment of outer-rise seismicity and its implications for the mechanics of oceanic lithosphere. *Geophysical Journal International*, 197(1), 63–89. <https://doi.org/10.1093/gji/ggu013>
- Dahlen, F. A. (1990). Critical taper model of fold-and-thrust belts and accretionary wedges. *Annual Review of Earth and Planetary Sciences*, 18(1), 55–99. <https://doi.org/10.1146/annurev.earth.18.050190.000415>

- Davis, D. M., & Engelder, T. (1985). The role of salt in fold-and-thrust belts. *Tectonophysics*, *119*(1–4), 67–88. [https://doi.org/10.1016/0040-1951\(85\)90033-2](https://doi.org/10.1016/0040-1951(85)90033-2)
- Dean, S. M., McNeill, L. C., Henstock, T. J., Bull, J. M., Gulick, S. P. S., Austin, J. A., et al. (2010). Contrasting decollement and prism properties over the Sumatra 2004–2005 earthquake rupture boundary. *Science*, *329*(5988), 207–210. <https://doi.org/10.1126/science.1189373>
- Faulkner, D. R., Mitchell, T. M., Behn, J., Hirose, T., & Shimamoto, T. (2011). Stuck in the mud? Earthquake nucleation and propagation through accretionary forearcs. *Geophysical Research Letters*, *38*, L18303. <https://doi.org/10.1029/2011GL048552>
- Fitch, T. J. (1972). Plate convergence, transcurrent faults, and internal deformation adjacent to Southeast Asia and Western Pacific. *Journal of Geophysical Research*, *77*(23), 4432–4460. <https://doi.org/10.1029/JB077i023p04432>
- Frederik, M. C. G., Gulick, S. P. S., Austin, J. A., Bangs, N. L. B., & Udrekh (2015). What 2-D multichannel seismic and multibeam bathymetric data tell us about the North Sumatra wedge structure and coseismic response. *Tectonics*, *34*, 1910–1926. <https://doi.org/10.1002/2014TC003614>
- Gabuchian, V., Rosakis, A. J., Bhat, H. S., Madariaga, R., & Kanamori, H. (2017). Experimental evidence that thrust earthquake ruptures might open faults. *Nature*, *545*(7654), 336–339. <https://doi.org/10.1038/nature22045>
- Graindorge, D., Klingelhoefer, F., Sibuet, J. C., McNeill, L., Henstock, T. J., Dean, S., et al. (2008). Impact of lower plate structure on upper plate deformation at the NW Sumatran convergent margin from seafloor morphology. *Earth and Planetary Science Letters*, *275*(3–4), 201–210. <https://doi.org/10.1016/j.epsl.2008.04.053>
- Gulick, S. P. S., Austin, J. A., McNeill, L. C., Bangs, N. L. B., Martin, K. M., Henstock, T. J., et al. (2011). Updip rupture of the 2004 Sumatra earthquake extended by thick indurated sediments. *Nature Geoscience*, *4*(7), 453–456. <https://doi.org/10.1038/ngeo1176>
- Hill, E. M., Borrero, J. C., Huang, Z. H., Qiu, Q., Banerjee, P., Natawidjaja, D. H., et al. (2012). The 2010 Mw 7.8 Mentawai earthquake: Very shallow source of a rare tsunami earthquake determined from tsunami field survey and near-field GPS data. *Journal of Geophysical Research*, *117*, B06402. <https://doi.org/10.1029/2012JB009159>
- Hoernle, K., Hauff, F., Werner, R., van den Bogaard, P., Gibbons, A. D., Conrad, S., & Muller, R. D. (2011). Origin of Indian Ocean Seamount Province by shallow recycling of continental lithosphere. *Nature Geoscience*, *4*(12), 883–887. <https://doi.org/10.1038/ngeo1331>
- Hupers, A., Torres, M. E., Owari, S., McNeill, L. C., Dugan, B., Henstock, T. J., et al. (2017). Release of mineral-bound water prior to subduction tied to shallow seismogenic slip off Sumatra. *Science*, *356*(6340), 841–844. <https://doi.org/10.1126/science.aal3429>
- Hyndman, R. D., Yamano, M., & Oleskevich, D. A. (1997). The seismogenic zone of subduction thrust faults. *Island Arc*, *6*(3), 244–260. <https://doi.org/10.1111/j.1440-1738.1997.tb00175.x>
- Ide, S., Baltay, A., & Beroza, G. C. (2011). Shallow dynamic overshoot and energetic deep rupture in the 2011 Mw 9.0 Tohoku-Oki earthquake. *Science*, *332*(6036), 1426–1429. <https://doi.org/10.1126/science.1207020>
- Jacob, J., Dymet, J., & Yatheesh, V. (2014). Revisiting the structure, age, and evolution of the Wharton Basin to better understand subduction under Indonesia. *Journal of Geophysical Research: Solid Earth*, *119*, 169–190. <https://doi.org/10.1002/2013JB010285>
- Kanamori, H. (1972). Mechanism of tsunami earthquakes. *Physics of the Earth and Planetary Interiors*, *6*(5), 346–359. [https://doi.org/10.1016/0031-9201\(72\)90058-1](https://doi.org/10.1016/0031-9201(72)90058-1)
- Konca, A. O., Avouac, J. P., Sladen, A., Meltzner, A. J., Sieh, K., Fang, P., et al. (2008). Partial rupture of a locked patch of the Sumatra megathrust during the 2007 earthquake sequence. *Nature*, *456*(7222), 631–635. <https://doi.org/10.1038/nature07572>
- Kopp, H., & Kukowski, N. (2003). Backstop geometry and accretionary mechanics of the Sunda margin. *Tectonics*, *22*(6), 1072. <https://doi.org/10.1029/2002TC001420>
- Kozdon, J. E., & Dunham, E. M. (2013). Rupture to the trench: Dynamic rupture simulations of the 11 March 2011 Tohoku earthquake. *Bulletin of the Seismological Society of America*, *103*(2B), 1275–1289. <https://doi.org/10.1785/0120120136>
- Lange, D., Tilmann, F., Henstock, T., Rietbrock, A., Natawidjaja, D., & Kopp, H. (2018). Structure of the central Sumatran subduction zone revealed by local earthquake travel-time tomography using an amphibious network. *Solid Earth*, *9*(4), 1035–1049. <https://doi.org/10.5194/se-9-1035-2018>
- Lavigne, F., Gomez, C., Giffo, M., Wassmer, P., Hoebreck, C., Mardiatno, D., et al. (2007). Field observations of the 17 July 2006 tsunami in Java. *Natural Hazards and Earth System Sciences*, *7*(1), 177–183. <https://doi.org/10.5194/nhess-7-177-2007>
- Lay, T., Ammon, C. J., Kanamori, H., Yamazaki, Y., Cheung, K. F., & Hutko, A. R. (2011). The 25 October 2010 Mentawai tsunami earthquake (Mw 7.8) and the tsunami hazard presented by shallow megathrust ruptures. *Geophysical Research Letters*, *38*, L06302. <https://doi.org/10.1029/2010GL046552>
- Li, L. Y., Cheung, K. F., Yue, H., Lay, T., & Bai, Y. F. (2016). Effects of dispersion in tsunami Green's functions and implications for joint inversion with seismic and geodetic data: A case study of the 2010 Mentawai Mw 7.8 earthquake. *Geophysical Research Letters*, *43*, 11,182–11,191. <https://doi.org/10.1002/2016GL070970>
- Liu, C. S., Curran, J. R., & McDonald, J. M. (1983). New constraints on the tectonic evolution of the eastern Indian Ocean. *Earth and Planetary Science Letters*, *65*(2), 331–342. [https://doi.org/10.1016/0012-821x\(83\)90171-1](https://doi.org/10.1016/0012-821x(83)90171-1)
- McCaffrey, R. (1991). Slip vectors and stretching of the Sumatran fore arc. *Geology*, *19*(9), 881–884. [https://doi.org/10.1130/0091-7613\(1991\)019<0881:Svasot>2.3.Co;2](https://doi.org/10.1130/0091-7613(1991)019<0881:Svasot>2.3.Co;2)
- McNeill, L. C., Dugan, B., Backman, J., Pickering, K. T., Poudereux, H. F. A., Henstock, T. J., et al. (2017). Understanding Himalayan erosion and the significance of the Nicobar Fan. *Earth and Planetary Science Letters*, *475*, 134–142. <https://doi.org/10.1016/j.epsl.2017.07.019>
- McNeill, L. C., Dugan, B., Petronotis, K. E., Backman, J., Bourlange, S., Chemale, F. Jr., et al. (2017). *Proceedings of the International Ocean Discovery Program; Sumatra subduction zone; Expedition 362 of the riserless drilling platform, Colombo, Sri Lanka, to Singapore; Sites U1480-U1481, 6 August-6 October 2016*. Washington, DC, United States: International Ocean Discovery Program.
- McNeill, L. C., & Henstock, T. J. (2014). Forearc structure and morphology along the Sumatra-Andaman subduction zone. *Tectonics*, *33*, 112–134. <https://doi.org/10.1002/2012TC003264>
- Moeremans, R., Singh, S. C., Mukti, M., McArdle, J., & Johansen, K. (2014). Seismic images of structural variations along the deformation front of the Andaman-Sumatra subduction zone: Implications for rupture propagation and tsunamigenesis. *Earth and Planetary Science Letters*, *386*, 75–85. <https://doi.org/10.1016/j.epsl.2013.11.003>
- Moore, G. F., Bangs, N. L., Taira, A., Kuramoto, S., Pangborn, E., & Tobin, H. J. (2007). Three-dimensional splay fault geometry and implications for tsunami generation. *Science*, *318*(5853), 1128–1131. <https://doi.org/10.1126/science.1147195>
- Moore, G. F., Shipley, T. H., Stoffa, P. L., Karig, D. E., Taira, A., Kuramoto, S., et al. (1990). Structure of the Nankai Trough accretionary zone from multichannel seismic-reflection data. *Journal of Geophysical Research*, *95*(B6), 8753–8765. <https://doi.org/10.1029/JB095iB06p08753>

- Mukti, M. M., Singh, S. C., Deighton, I., Hananto, N. D., Moeremans, R., & Permana, H. (2012). Structural evolution of backthrusting in the Mentawai Fault Zone, offshore Sumatran forearc. *Geochemistry, Geophysics, Geosystems*, *13*, Q12006. <https://doi.org/10.1029/2012GC004199>
- Natawidjaja, D. H., Sieh, K., Chlieh, M., Galetzka, J., Suwargadi, B. W., Cheng, H., et al. (2006). Source parameters of the great Sumatran megathrust earthquakes of 1797 and 1833 inferred from coral microatolls. *Journal of Geophysical Research*, *111*, B06403. <https://doi.org/10.1029/2005JB004025>
- Natawidjaja, D. H., Sieh, K., Ward, S. N., Cheng, H., Edwards, R. L., Galetzka, J., & Suwargadi, B. W. (2004). Paleogeodetic records of seismic and aseismic subduction from central Sumatran microatolls, Indonesia. *Journal of Geophysical Research*, *109*, B04306. <https://doi.org/10.1029/2003JB002398>
- Newman, A. V., Hayes, G., Wei, Y., & Convers, J. (2011). The 25 October 2010 Mentawai tsunami earthquake, from real-time discriminants, finite-fault rupture, and tsunami excitation. *Geophysical Research Letters*, *38*, L05302. <https://doi.org/10.1029/2010GL046498>
- Noda, H., & Lapusta, N. (2013). Stable creeping fault segments can become destructive as a result of dynamic weakening. *Nature*, *493*(7433), 518–521. <https://doi.org/10.1038/nature11703>
- Pedley, K. L., Barnes, P. M., Pettegaa, J. R., & Lewis, K. B. (2010). Seafloor structural geomorphic evolution of the accretionary frontal wedge in response to seamount subduction, Poverty Indentation, New Zealand. *Marine Geology*, *270*(1–4), 119–138. <https://doi.org/10.1016/j.margeo.2009.11.006>
- Philibosian, B., Sieh, K., Avouac, J. P., Natawidjaja, D. H., Chiang, H. W., Wu, C. C., et al. (2014). Rupture and variable coupling behavior of the Mentawai segment of the Sunda megathrust during the supercycle culmination of 1797 to 1833. *Journal of Geophysical Research: Solid Earth*, *119*, 7258–7287. <https://doi.org/10.1002/2014JB011200>
- Philibosian, B., Sieh, K., Avouac, J. P., Natawidjaja, D. H., Chiang, H. W., Wu, C. C., et al. (2017). Earthquake supercycles on the Mentawai segment of the Sunda megathrust in the seventeenth century and earlier. *Journal of Geophysical Research: Solid Earth*, *122*, 642–676. <https://doi.org/10.1002/2016JB013560>
- Polet, J., & Kanamori, H. (2000). Shallow subduction zone earthquakes and their tsunamigenic potential. *Geophysical Journal International*, *142*(3), 684–702. <https://doi.org/10.1046/j.1365-246x.2000.00205.x>
- Prawirodirjo, L., McCaffrey, R., Chadwell, C. D., Bock, Y., & Subarya, C. (2010). Geodetic observations of an earthquake cycle at the Sumatra subduction zone: Role of interseismic strain segmentation. *Journal of Geophysical Research*, *115*, B03414. <https://doi.org/10.1029/2008JB006139>
- Qin, Y. F., & Singh, S. C. (2017). Detailed seismic velocity of the incoming subducting sediments in the 2004 great Sumatra earthquake rupture zone from full waveform inversion of long offset seismic data. *Geophysical Research Letters*, *44*, 3090–3099. <https://doi.org/10.1002/2016GL072175>
- Qin, Y. F., & Singh, S. C. (2018). Insight into frontal seismogenic zone in the Mentawai locked region from seismic full waveform inversion of ultralong offset streamer data. *Geochemistry, Geophysics, Geosystems*, *19*, 4342–4365. <https://doi.org/10.1029/2018GC007787>
- Satake, K., Nishimura, Y., Putra, P. S., Gusman, A. R., Sunendar, H., Fujii, Y., et al. (2013). Tsunami source of the 2010 Mentawai, Indonesia earthquake inferred from tsunami field survey and waveform modeling. *Pure and Applied Geophysics*, *170*(9–10), 1567–1582. <https://doi.org/10.1007/s00024-012-0536-y>
- Sieh, K., Natawidjaja, D. H., Meltzner, A. J., Shen, C. C., Cheng, H., Li, K. S., et al. (2008). Earthquake supercycles inferred from sea-level changes recorded in the corals of West Sumatra. *Science*, *322*(5908), 1674–1678. <https://doi.org/10.1126/science.1163589>
- Spinelli, G. A., & Underwood, M. B. (2004). Character of sediments entering the Costa Rica subduction zone: Implications for partitioning of water along the plate interface. *Island Arc*, *13*(3), 432–451. <https://doi.org/10.1111/j.1440-1738.2004.00436.x>
- Suppe, J. (1983). Geometry and kinematics of fault-bend folding. *American Journal of Science*, *283*(7), 684–721. <https://doi.org/10.2475/ajs.283.7.684>
- Ulutas, E. (2013). Comparison of the seafloor displacement from uniform and non-uniform slip models on tsunami simulation of the 2011 Tohoku-Oki earthquake. *Journal of Asian Earth Sciences*, *62*, 568–585. <https://doi.org/10.1016/j.jseas.2012.11.007>
- von der Borch, C. C., Sclater, J. G., Gartner, S. Jr., Hekinian, R., Johnson, D. A., McGowran, B., et al. (1974). *Initial reports of the Deep Sea Drilling Project, covering Leg 22 of the cruises of the drilling vessel Glomar Challenger; Darwin, Australia to Colombo, Ceylon, January–March 1972*. Ocean Drilling Program, College Station, TX, United States: Texas A & M University.
- Wang, K. L., & Hu, Y. (2006). Accretionary prisms in subduction earthquake cycles: The theory of dynamic Coulomb wedge. *Journal of Geophysical Research*, *111*, B06410. <https://doi.org/10.1029/2005JB004094>
- Yue, H., Lay, T., Li, L. Y., Yamazaki, Y., Cheung, K. F., Rivera, L., et al. (2015). Validation of linearity assumptions for using tsunami waveforms in joint inversion of kinematic rupture models: Application to the 2010 Mentawai Mw 7.8 tsunami earthquake. *Journal of Geophysical Research: Solid Earth*, *120*, 1728–1747. <https://doi.org/10.1002/2014JB011721>
- Yue, H., Lay, T., Rivera, L., Bai, Y. F., Yamazaki, Y., Cheung, K. F., et al. (2014). Rupture process of the 2010 Mw 7.8 Mentawai tsunami earthquake from joint inversion of near-field hr-GPS and teleseismic body wave recordings constrained by tsunami observations. *Journal of Geophysical Research: Solid Earth*, *119*, 5574–5593. <https://doi.org/10.1002/2014JB011082>
- Zhang, L. F., Liao, W. L., Li, J. G., & Wang, Q. L. (2015). Estimation of the 2010 Mentawai tsunami earthquake rupture process from joint inversion of teleseismic and strong ground motion data. *Geodesy and Geodynamics*, *6*(3), 180–186. <https://doi.org/10.1016/j.geog.2015.03.005>